Bulletin of the Seismological Society of America, Vol. 97, No. 1A, pp. S1–S, January 2007, doi: 10.1785/0120050616

Rupture Properties of the Giant Sumatra Earthquake Imaged by Empirical Green's Function Analysis

by Martin Vallée

Abstract Empirical green's function (EGF) analysis has remained little used to image the rupture properties of the giant 26 December 2004 Sumatra earthquake. The 2 November 2002 foreshock (M_w 7.2), close to the mainshock epicenter, gives us the opportunity to use its waveforms to empirically simulate the Rayleigh-wave propagation of the Sumatra earthquake. We first show that the exceptional size of the Sumatra earthquake does not prevent use of the EGF technique. Four aftershocks (M_w 5.9–6.1), distributed along the Sumatra–Andaman trench, are shown to have consistent Rayleigh waves for periods between 100 and 200 sec. At a lower frequency, we present two large earthquakes of the Mexican subduction zone (M_w 7.2–7.3, close to the selected EGF magnitude) for which long-period Green's functions (100–2000 sec) remain very similar, even if event epicenters are separated by about 650 km. This justifies the possibility of using the 2002 foreshock as an EGF for the whole rupture process of the Sumatra earthquake and shows more generally the very broad range of application of EGF technique. Then, a specific analysis reveals that seismic moment magnitude is close to 9.1 (seismic moment equal to 5.6×10^{22} N m). Moment release analysis along the Sumatra–Andaman trench shows two main slip episodes: one next to the northern extremity of Sumatra (~20-m slip) and the other one along the Nicobar Islands (~10-m slip), with a global extent of 1150–1200 km. Rupture velocity varies between values around 2.5 km/sec in the first half of the rupture and values closer to 2 km/sec in the second half. Total duration imaged by Rayleigh waves is 580 sec ($\pm$20 sec) and no activity of the fault is found in the time scale between 600 and 2000 sec. In the hypothesis of even longer timescale slip, this phenomenon would be of the order of 10%–20% of the global moment and likely restricted to the Andaman Islands.

Introduction

On 26 December 2004, the giant Sumatra earthquake and especially its associated tsunami devastated a large part of Southeast Asia. This exceptional earthquake has stimulated active research in different areas of geophysics, which has lead to a better description of the phenomenon. Although early earthquake source analyses of teleseismic body waves (Yagi, 2004; Yamanaka, 2004; Ji, 2005) modeled a rupture length of a few hundred of kilometers, it soon appeared that this value had been strongly underevaluated. The first and simplest clue of a very long rupture came from aftershock locations that delineate a 1300-km-long zone (Fig. 10). First field observations (Department of Civil Engineering, 2005) and Global Positioning System (GPS) results (CESS Seismology Research Group, 2005; Survey of India, 2005) from the Andaman Islands also required that large fault slip took place close to these islands. Then, analyses of high-frequency body waves (Lomax, 2005; Ni *et al.*, 2005) or array analyses (de Groot-Hedlin, 2005; Guilbert *et al.*, 2005; Ishii *et al.*, 2005; Krüger and Ohrnberger, 2005) confirmed that rupture lasted at least 8 min and ruptured most parts of the subduction zone between Sumatra and Myanmar.

At the other extremity of the seismic frequency band, ultralong periods, normal modes recorded by worldwide seismometers have provided complementary information on the event. Analyses by Park *et al.* (2005), Stein and Okal (2005), and Lambotte *et al.* (2007) have shown a M_w 9. The Harvard Centroid moment tensor (CMT) value (Harvord Seismology, 2004) has likely been underestimated. Magnitude as large as 9.3 has been proposed by Stein and Okal (2005). Using splitting of normal modes, Lambotte *et al.* (2007) have identified both a long duration (~500 sec) and extent (~1220 km) of the earthquake.

Finally, detailed seismological (Ammon *et al.*, 2005; Lay *et al.*, 2005) and geodetical analyses (Vigny *et al.*, 2005) have precisely determined the dimensions and properties of the rupture. In particular, very large GPS displacements all

over the Southeast Asia peninsula obtained by Vigny *et al.* (2005) shows that fault slip occurred in a large part of the subduction zone, between 3° N and 12° N.

Thanks to this broad range of analyses there is today little doubt on the rupture extent of the Sumatra earthquake. Yet, some other characteristics are still debated, particularly the real duration and magnitude of the event. While much of the data can be explained by a ~550-sec-long source (Park *et al.*, 2005), the hypothesis of a much longer source is still considered. One of the main elements in favor of such an hypothesis comes from the location of the tsunamigenic source by backpropagating the arrival times of the waves in the Bengal Bay (Lay *et al.*, 2005). This delineates a 800-km-long zone and does not include the Andaman Islands, where large static displacements have been observed. The slow-slip hypothesis is still questioned because according to Vigny *et al.* (2005), no movement is seen at GPS stations in Southeast Asia for timescales longer than 15 mn. On the other hand, Banerjee *et al.* (2005), by comparing seismological and geodetical slip models, have proposed that there is a 25%–35% moment deficit in the seismic models. The missing displacement would be due to slip occuring at periods longer than 1 hr, not able to efficiently generate neither seismic nor tsunami waves.

Magnitude is also discussed because very long period waves are required to adequately estimate the moment of such a large event. Thus, values estimated from body or short-period surface waves (<300 sec) likely underestimate the global moment. Normal modes, with periods of several thousands of seconds, have a higher potential to estimate moment magnitude (Park *et al.*, 2005; Stein and Okal, 2005; Lambotte *et al.*, 2007). Unfortunately, the measure is very sensitive on the earthquake dip, and dip values of 15° or 8° would respectively lead to moment magnitudes equal to 9.1 or 9.3. Finally, geodesy has measured displacements consistent with magnitudes bigger than 9, but the conversion to seismic moment is not direct because of trade-off with dip angle and rigidity structure (Banerjee *et al.*, 2005).

As another way to analyse this major event, I propose to use a smaller earthquake (M_w 7.2) to image the mainshock rupture, using the EGF approach. I will show that such an analysis can be adapted to this very long earthquake. First Rayleigh waves of four M_w ~6 aftershocks distributed along the Sumatra–Andaman trench will be shown to be consistent in the period band 100–200 sec. To examine the consistency at lower frequency, we will use two earthquakes of the Mexican subduction zone (M_w 7.2–7.3) and show waveforms similarity for periods between 100 and 2000 sec. Then a specific study on the optimal magnitude of the Sumatra earthquake is done before describing the rupture process of this unique event.

Empirical Green's Function (EGF) Approach

Generalities and Location Errors

The idea of the EGF method, already present in the late 1960s (Aki, 1967) and later applied to seismic source analysis (Hartzell, 1978), uses the fact that earthquake source process is similar regardless of the magnitude. Therefore a small earthquake (called EGF) can be used to model a big one, provided both events are similar in terms of mechanism and location. This approach has been subsequently used and developed by Mueller (1985), Fukuyama and Irikura (1986), Mori and Frankel (1990), Ammon *et al.* (1993), Velasco *et al.* (1994), Ihmlé (1996), Courboulex *et al.* (1996), Bertero *et al.* (1997), and Vallée (2004). It has been shown that the EGF optimal magnitude is about 1°–2° smaller than the mainshock, in order to keep a good signal-to-noise ratio at low frequency. In the active Sumatra subduction zone, the best candidate is a M_w 7.2 earthquake that occurred in November 2002 (Figs. 7 and 10).

In a schematic way, seismic waves recorded at a distant seismic station contain two linear contributions: one coming from the earthquake's apparent moment rate and the other coming from Earth propagation. The Earth propagation complexity is present in a similar manner for both the EGF and the mainshock. Thus it is possible by a deconvolution to extract the apparent moment rate function (also called relative source time function [RSTF]) of the mainshock. Technically, the same wavetypes, at the same seismic stations, have to be studied for both earthquakes. In this case of a very large earthquake, surface waves constitute the best choice, because (1) they are sensitive to long periods and (2) they do not suffer from the wave mixing of body waves. In fact, for such a long-duration earthquake, individual body waves (*P, PP, S, SS*) are not separated and thus cannot be directly used (e.g., Ni *et al.*, 2005).

Of course, errors come from the fact that the propagation model given by the EGF is not perfect. For the Sumatra earthquake, with extent bigger than 1000 km, the most obvious error origin is the source location difference, in the later part of the rupture, between mainshock and EGF. Variations of trench azimuth and of age of the subducted lithosphere between north Sumatra and Andaman Islands may also lead to a significant modification of the Green's function. To examine quantitatively these potential problems, we can look at waveforms generated by similar but distant earthquakes. Unfortunately, it is not possible to directly compare our selected EGF (M_w 7.2) with other earthquakes in the Sumatra subduction zone. Indeed, except in the coda of the mainshock, no large thrust earthquake (M_w >6.4) occurred in the Nicobar–Andaman region. Thus we propose two analyses to provide insights on the waveforms similarity as a function of the interdistance between events. First we compare moderate magnitude (M_w 5.9–6.1) aftershocks of the Sumatra event. In this magnitude range, four thrust earthquakes, distributed from south to north along the Sumatra–Andaman trench have been selected: the M_w 5.9 31 January 2006 (2.70° N, 96.07° E, centroid depth 23 km); M_w 5.9 1 May 2005 (5.49° N, 94.39° E, centroid depth 33 km), M_w 5.9 1 April 2005 (10.67° N, 92.36° E, centroid depth 24 km), and M_w 6.1 02 March 2006 (11.90° N, 92.41° E, centroid depth 20 km) events. Their locations and mech-

anisms can be seen in Figure 10. The 31 January 2006 earthquake is very close, in terms of location and mechanism, to the 2 November 2002 EGF. Therefore, waveforms comparison between this event and the other ones will give meaningful elements on the validity of our EGF hypothesis.

We used data from worldwide FDSN broadband stations at epicentral distances between 55° and 125°. We have avoided closer stations, where the effect of earthquakes centroid difference is larger, as well as further stations, where R2 Rayleigh waves arrive soon after the end of R1 Rayleigh wave train. Figure 1 shows vertical seismograms for the four aftershocks, recorded at 12 stations with various azimuths. The thicker lines correspond to the earthquakes closer to the selected EGF. Six of the 10 stations later used in our study (namely FFC, PET, TAU, LSZ, PAB, ARU) are present in this analysis. The other ones, mainly located on oceanic islands (KIP, KWAJ, CRZF), cannot be compared because of low signal-to-noise ratio due to the relatively small aftershocks magnitude. Data has been windowed in the R1 Rayleigh-waves window, and seismograms initial time is based on the same phase velocity, corresponding to the arrival of Rayleigh waves at each station. Data has been bandpassed between 100 and 200 sec, because shorter periods are logically different due to the centroid difference and longer periods are not excited enough for these M_w 6.0 earthquakes.

Figure 1 shows that Rayleigh waves of the 5 January 2005 and of the 31 January 2006 earthquake (thickest lines) remain similar at most stations. This illustrates that in the analyzed frequency band (100–200 sec), the distance between events (360 km), the strike variation (~30°), the depth difference (~10 km), and the nature change of the subducted

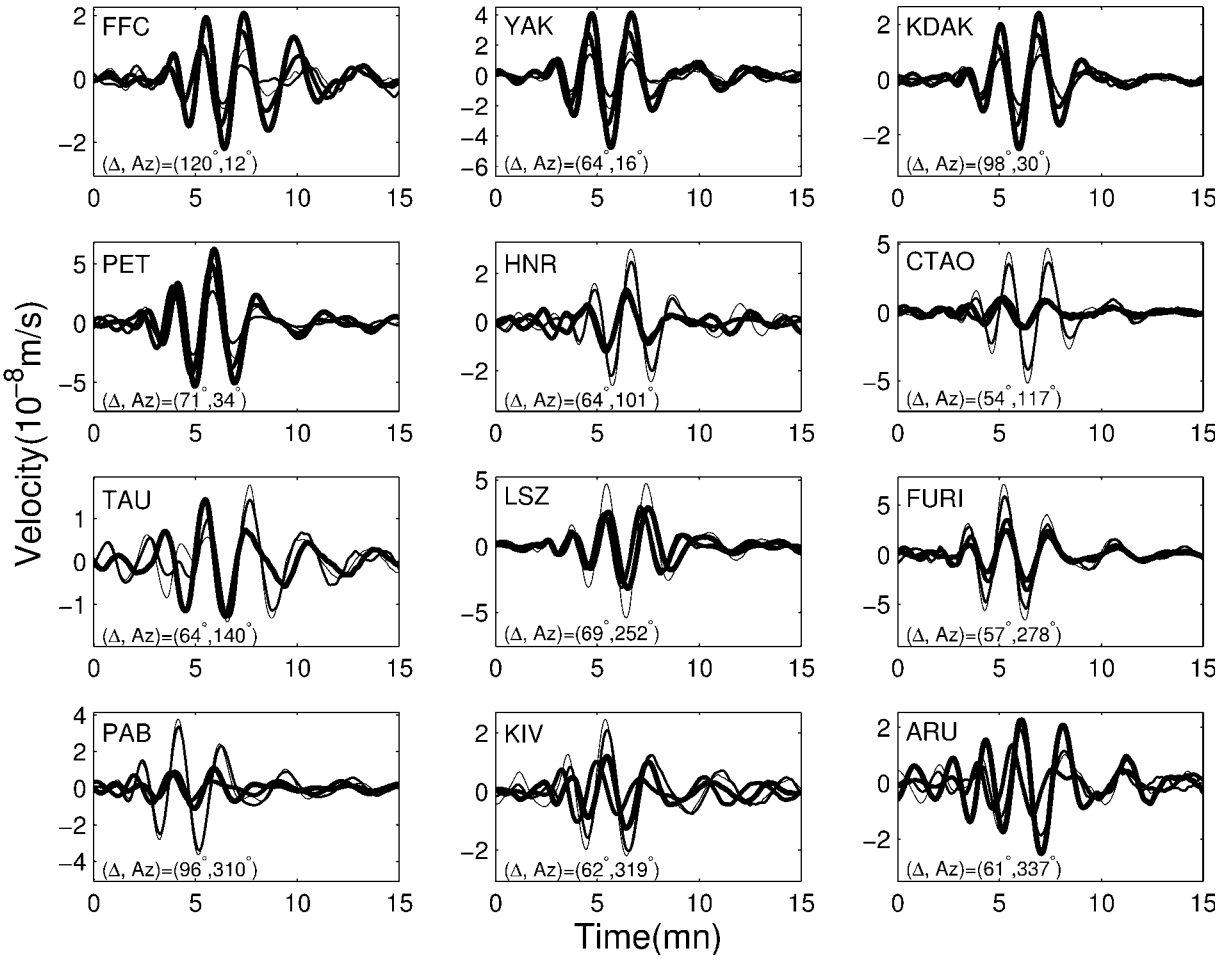

Figure 1. Comparison of Rayleigh waves recorded at the same stations for four earthquakes of the Sumatra–Andaman subduction zone. Thick lines refer to earthquakes close to the 2 November 2002 EGF. By order of decreasing thickness, lines refer to the 31 January 2006, 5 May 2005, 4 January 2005, and 3 February 2006 earthquakes (see their locations and mechanisms in Fig. 10). Rayleigh waves of the 5 January 2005 earthquake are noisy at TAU station and are not presented here. Name, epicentral distance (Δ), and azimuth (θ) are shown in the each subfigure. Vertical seismograms, aligned on the arrival of the Rayleigh waves, have been bandpass filtered between 100 and 200 sec.

lithosphere only have a small influence on the shape of the Green's function. Even if it logically decreases, the Rayleigh waves consistency remains for the two other earthquakes (4 January 2005 and 3 February 2006), respectively located 970 km and 1100 km from the 31 January 2006 earthquake. Among the selected stations for the following analysis, correlation is good at FFC, PET, TAU, and LSZ and somewhat lower at ARU and PAB where amplitude of Rayleigh waves varies between earthquakes. This analysis shows that even in a very long and complex subduction zone, the EGF analysis is meaningful if we limit the study to long periods.

To examine more specifically the limitation at long periods, we need to refer to earthquakes of similar magnitude as our selected EGF (M_w 7.2). As explained before, a pair of such earthquakes does not exist in the Sumatra–Andaman subduction zone. Looking at other regions, we have found that Mexican subduction generated, in 1993 and 1995, two earthquakes suitable for this waveform comparison. On 10 September 1993, a M_w 7.2 earthquake occurred in the Chiapas region and on 14 September 1995, a M_w 7.3 earthquake occurred in the Guerrero region (Fig. 2). Both events have similar mechanisms and a centroid location difference of about 650 km (Harvard Seismology, 2004). Following the same analysis as for Sumatra aftershocks, we present in Figure 3 vertical Rayleigh waves generated by the two earthquakes at 16 stations of the global network. In this case, thanks to the better signal-to-noise ratio, waveforms remain nearly identical in the whole period band 100–2000 sec.

These examples show, by a direct use of seismic data, that it is justified to use only one EGF to model Earth propagation, even for a very long and complex rupture zone. We have shown that periods longer that 100 sec remain reliable for most part of Sumatra earthquake rupture zone. At the other extremity of the frequency band, the analysis of M_w 7.2 earthquakes reveals that periods as long as 2000 sec are above the noise level. Subsequent analysis will therefore be done in the broad period range between 100 and 2000 sec.

Description of Deconvolution Method

Even if it has been illustrated that the entire rupture extent can be taken into account by only one EGF, it remains useful to use stabilization techniques to obtain the most reliable information about the source process. In particular, methods including corrections for mechanism difference and EGF duration (Ihmlé, 1996; Ihmlé and Ruegg, 1997) or positivity and temporal constraints on the RSTFs (Bertero *et al.*, 1997; Courboulex *et al.*, 1996) have been developed. I have shown for the very large 23 June 2001 Peru earthquake (M_w 8.4) that global rupture characteristics can be efficiently retrieved, provided some physical constraints on the RSTFs are respected (Vallée, 2004). Namely, positivity, causality, finite duration, and equal moment ratio constraints are shown to be very efficient to extract reliable moment rates. The equal moment ratio constraint simply states that the area of the RSTF has to be the same at all stations because it represents the moment ratio between the mainshock and the EGF. Details about the technique itself are not recalled here and can be found in Vallée (2004) and Vallée and Bouchon (2004).

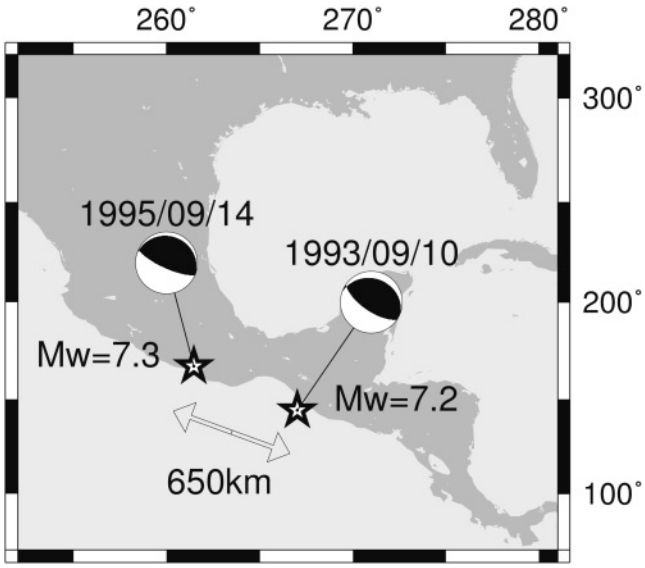

Figure 2. Map of Central America showing location of the Chiapas (10 September 1993) and Guerrero (14 September 1995) earthquakes used in this study. Values of moment magnitudes, focal mechanisms, and centroid locations (stars) are taken from Harvard CMT (Harvard Seismology, 2004).

As an illustration for the Sumatra earthquake case, Figure 4 shows the analysis process for broadband station TAU (Tasmania) of the global network. Both EGF and mainshock Rayleigh waves have been prefiltered between 100 and 2000 sec to take into account the limitations underlined in the previous part. Magnitude of the Sumatra mainshock and EGF are respectively taken equal to 9.1 and 7.2 (Harvard CMT value), yielding a moment ratio of 620. Figure 4a first determines the optimal RSTF duration. To do so, we present the misfit between the real mainshocks and the reconstituted mainshock obtained by reconvolution of the RSTF with the EGF, as a function of the allowed duration of the RSTF. This misfit is a good indicator of the quality of the obtained deconvolution. The time at which the function becomes flat (ellipse) gives the simplest (i.e., shortest) RSTF able to well describe the seismic source. Figure 4b shows the RSTF corresponding to this optimal duration, and finally, Figure 4c presents a comparison between the real mainshock and the reconstituted mainshock for the preferred RSTF. At TAU station (azimuth 141°), the optimal RSTF duration is 840 sec long (Fig. 4a), which traduces the antidirective station position with respect to Sumatra earthquake propagation. The corresponding RSTF (Fig. 4b), which is able to reproduce very well the mainshock waveforms (Fig. 4c), gives interesting information on the temporal and spatial moment release of the event. This information is used later in the definition of the earthquake rupture process.

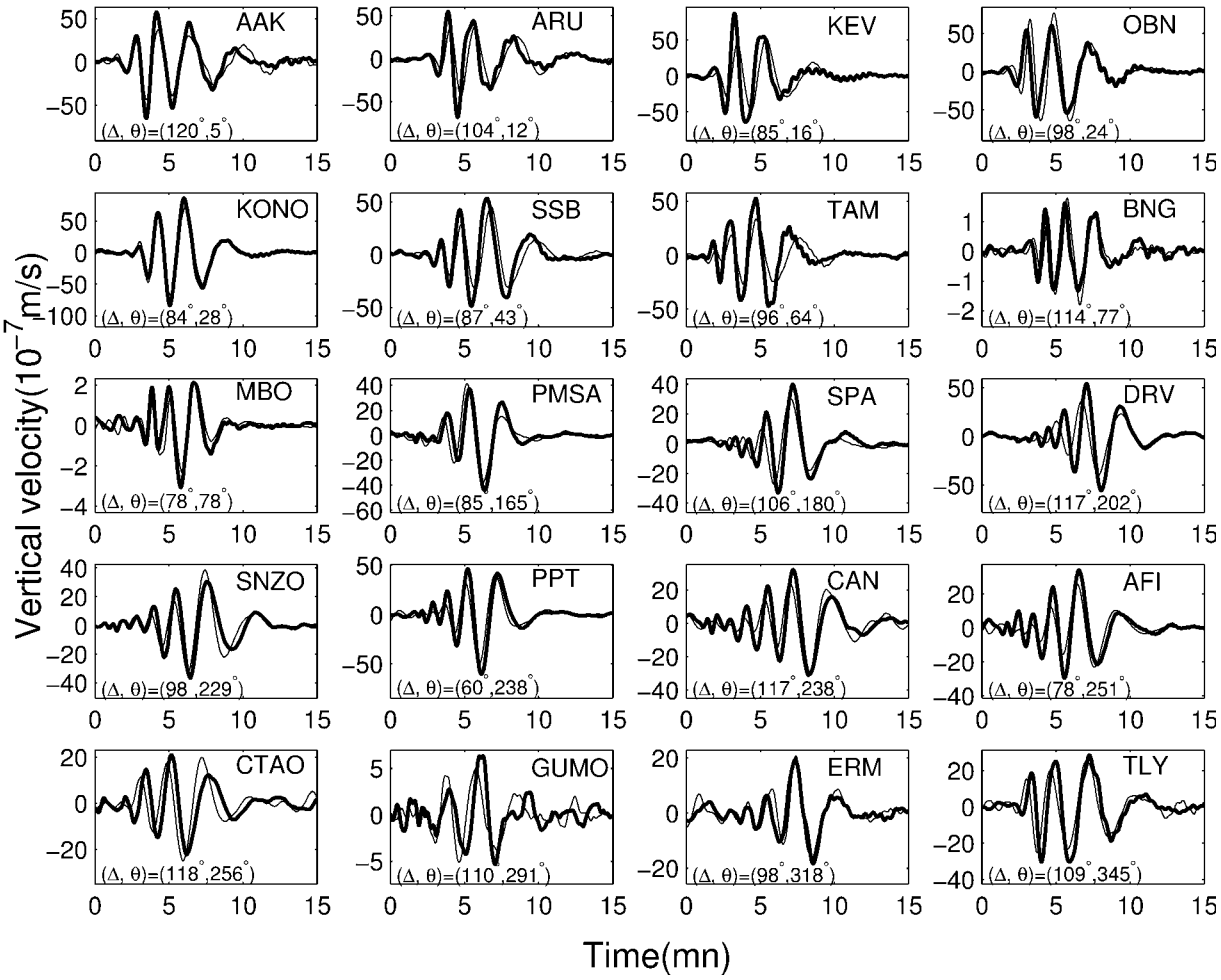

Figure 3. Comparison of Rayleigh waves recorded at the same stations for both Chiapas (thin lines) and Guerrero (thick lines) earthquakes. Station name, epicentral distance (Δ), and azimuth (θ) are shown in the each subfigure. Vertical seismograms, aligned on the arrival of the Rayleigh waves, have been bandpass filtered between 100 and 2000 sec.

Application to the Determination of Sumatra Earthquake Seismic Moment

Before going into the details of the rupture process, we can use the deconvolution method in another way to refine the seismic moment of the mainshock. In fact, rather than considering the moment ratio as a constraint, we can do an optimization of this parameter by searching which moment ratio leads to the best RSTFs (by best RSTFs, we mean as before the shortest RSTFs for which the convolution with the EGF will be the closest from the mainshock waveforms). This offers a new way to define the seismic moment of this unique earthquake.

Therefore, we consider five values of the Sumatra earthquake moment magnitude (8.9, 9.0, 9.1, 9.2, 9.3), ranging over the possible magnitude values. The EGF magnitude is fixed to the 7.2 Harvard CMT value (moment of 9×10^{19} N m), because Harvard CMT technique based on long-period body and mantle waves is very reliable for this type of magnitude. For each of possible mainshock magnitude, we use the deconvolution technique described in the previous section. Figure 5 presents, at the two stations COR and KONO, the equivalent of Figure 4a for station TAU. But rather than representing only the misfit for a mainshock magnitude equal to 9.1, we show the five curves corresponding to the five hypotheses for Sumatra seismic moment. For station COR, all moment hypothese lead to a similar quality RSTF if the allowed duration is very long. Yet the best misfit level is reached for duration of about 400 sec for magnitudes equal to 8.9, 9.0., and 9.1 whereas a duration longer than 600 sec is required to obtain a good RSTF for magnitudes 9.2 and 9.3. We thus consider that magnitudes equal to 9.2 or 9.3 are not optimal because they can give a good RSTF only if very long periods, little excited by surface waves, are added to the RSTF. For station KONO, the conclusion is even more direct: magnitudes equal to 8.9 or 9.0 are not able to yield a satisfactory RSTF whatever the duration. Figure 6

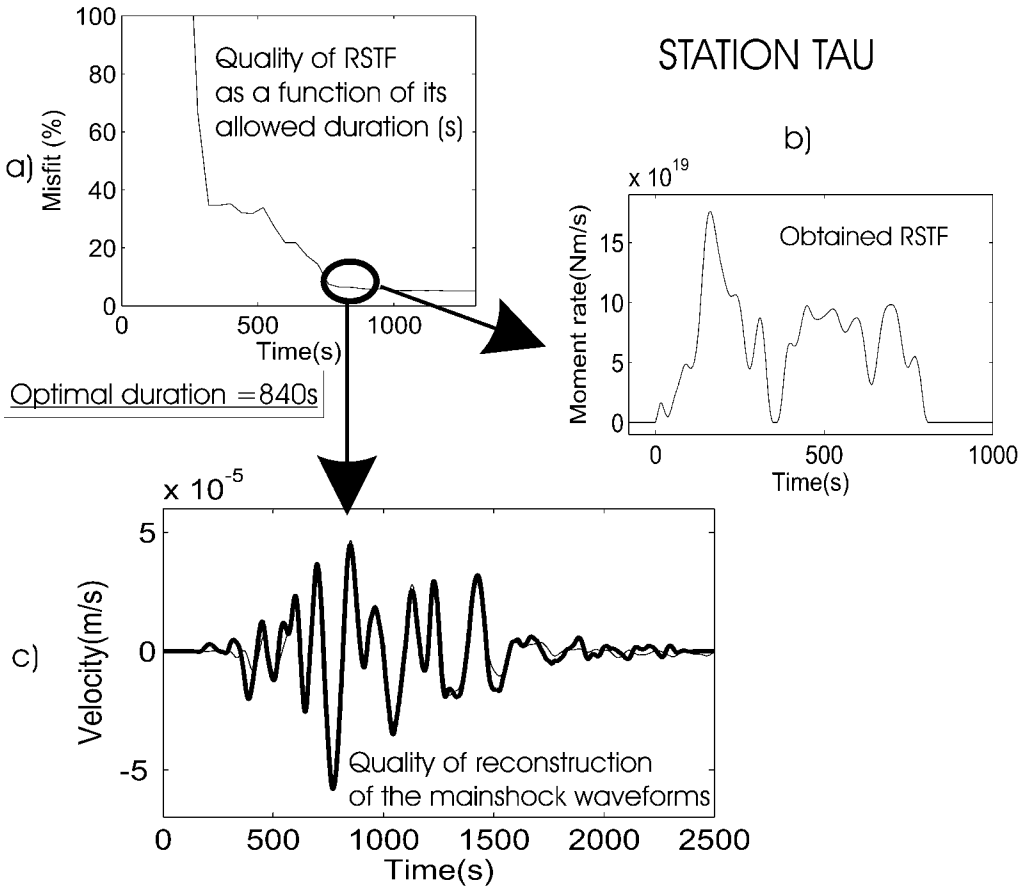

Figure 4. Illustration of the deconvolution technique for Rayleigh waves at station TAU (Tasmania). Deconvolution is done with four constraints (causality, positivity, finite duration, and moment ratio fixed to 620). First we impose a very short duration of the RSTF, which logically leads to a bad reconstruction of the mainshock waveforms by reconvolution with the EGF. The error associated with this reconstruction is our definition of the misfit used in (a). Then we allow a longer and longer duration that decreases the misfit in (a). When we reach an allowed duration of 840 sec the misfit is low (~6%) and cannot be improved further by a longer allowed duration. Therefore we select the 840-sec-long RSTF, presented in (b), as the most likely RSTF. The convolution of this RSTF with the EGF yields the thin line in (c), whereas the thick line is the real mainshock waveform.

shows the results of a similar analysis for 18 stations of worldwide networks (IU, II, Geoscope, TGRS). Based on the criteria described for stations COR and KONO, the horizontal line represents, at each station, the possible values for earthquake magnitude. The observation of this figure reveals that a seismic moment magnitude equal to 9.1 (moment of 5.6×10^{22} N m) is the optimal value of the giant Sumatra earthquake, as seen by broadband Rayleigh waves (100–2000 sec).

Imaging of Rupture Properties

Using the M_w 9.1 value determined in the previous section, the stabilized deconvolution technique is used to retrieve RSTFs at stations of the global networks. Based on well-distributed azimuthal coverage, 10 RSTFs are selected and presented in Figure 7. Some striking features may immediately be commented on: the RSTFs durations vary from 300 sec in Europe (PAB and ARU) up to 900 sec in Antarctica (SBA). Such a behavior is expected because the earthquake propagation from southeast to northwest leads to an energy concentration in the northwest direction.

To estimate more quantatively the rupture process of Sumatra earthquake, a one-dimensional model of the earthquake is considered, in which seismic moment is released along the trench. This line-source model, where trench curvature has been taken into account, is shown in Figure 10. Assuming such geometry, the RSTF F_θ observed in an azimuth θ can be written as the integral along the fault of length L:

$$F_\theta(t) = \int_0^L f_{m,d}(x, t - T_r(x,V_r) + D(x,\theta,\theta_f,V_\phi))dx, \quad (1)$$

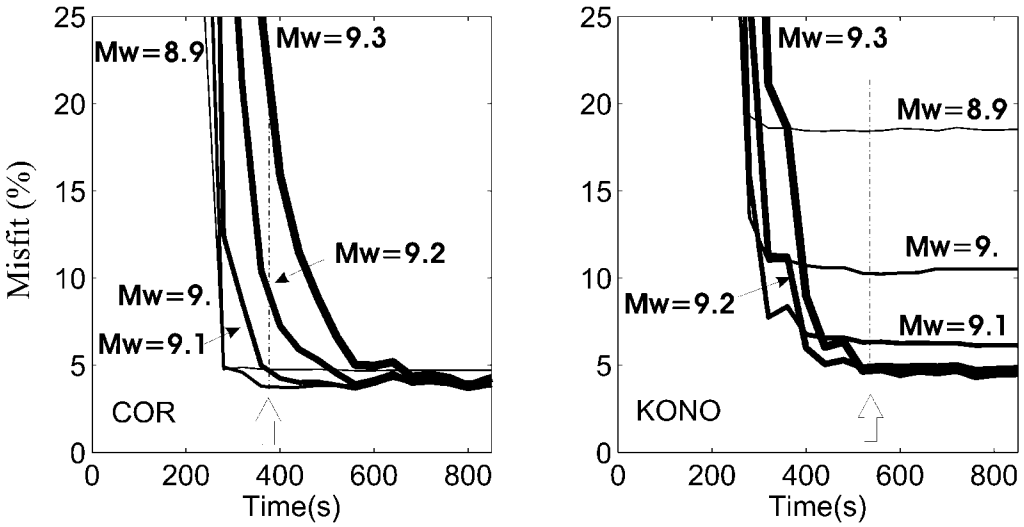

Figure 5. Illustration of the magnitude discrimination at stations COR and KONO. The line thicknesses refer to magnitude hypotheses, between 8.9 and 9.3. In both sub figures, the evolution of the misfit as a function of the RSTF allowed duration is presented (see Fig. 4a) for more details). At COR, the optimal RSTF duration is about 400 sec (arrow). Magnitudes 9.2 and 9.3 are able to produce a good RSTF, but only if a longer duration, including very low frequencies little excited by Rayleigh waves, is permitted. At KONO station, magnitudes 8.9 and 9.0 produce an agreement with data significantly less good than larger magnitudes. This illustrates that magnitude 9.1 is the most plausible magnitude of Sumatra earthquake. This is confirmed with a larger number of stations in Figure 6.

where f, the local source time function (i.e., defining the moment rate of a point located at distance x from hypocenter) is parametrized by moment per unit length m and moment per unit length duration d. Temporal contributions due to propagation time T_r (related to rupture velocity V_r) and spatial shift between source and station (D function) have to be taken into account. D is dependent on station azimuth θ, fault azimuth θ_f, and phase velocity V_φ; it can be simply evaluated knowing that D is simply equal to $(x \cos(\theta\text{-}\theta_f)/V_\varphi)$ for a constant azimuth segment fault. Rayleigh-wave phase velocity V_ϕ is averaged to 3.7 km/sec by observation of the arrival time of the EGF most energetic Rayleigh waves.

Equation (1) gives us a useful relation between the observation F_θ and source parameters m, V_r, and d; d takes into account time between slip initiation and slip termination at a point of the fault as well as time to propagate along the half-width of the fault. With slip in the range 5–20 m, slip velocity around 1 m/sec (Heaton, 1990), fault width of the order of 100–200 km, and rupture velocity of 2–3 km/sec, typical values for d are of the order of 25–60 sec.

Thus we keep as unknowns of equation (1) the moment per unit length m and the rupture velocity V_r on the fault. To retrieve these parameters, the 1500-km-long fault is discretized in 100-km-long segments. Slip is constrained to be zero at the last point of the fault, and local rupture velocity can vary between 1.4 and 3.3 km/sec. To define the 30 parameters of this optimization problem, residuals between observed RSTFs and RSTFs calculated with equation (1) have to be minimized. A small smoothing constraint is introduced for rupture velocity to reduce the instability of this parameter at fault points where seismic moment is low.

Before inversion, observed RSTFs have been smoothed to (1) reduce the effect of unreliable frequencies and (2) take into account the spatial sampling of the fault ($s_f = 100$ km), which prevents modeling high frequencies. Because of rupture propagation toward the north, smoothing has to be dependent on the azimuth, and its value is estimated by the following equation:

$$\text{Smooth} = 2s_f\left(\frac{1}{\bar{V}_r} - \frac{\cos(\theta - \bar{\theta}_f)}{V_\varphi}\right), \qquad (2)$$

where $\bar{V}_r$ and $\bar{\theta}_f$, average values of rupture velocity and fault azimuth, respectively, are here approximated to 2.25 km/sec and 342°. Using equation (2), smoothing values range from 26 sec for $\theta = 337°$ (ARU, directive station) to 134 sec for $\theta = 168°$ (SBA, antidirective station). The observed smoothed RSTFs are presented in Figure 8 (thick lines).

The inverse problem is then solved with the neighborhood algorithm (NA) (Sambridge, 1999). To estimate model uncertainties, we repeat the use of NA with different parameters, including variation of d in the range 25–60 sec and modification of rupture velocity smoothing constraint. Based on 12 NA runs, the averages and standard errors of moment per unit length and rupture velocity are presented in Figure

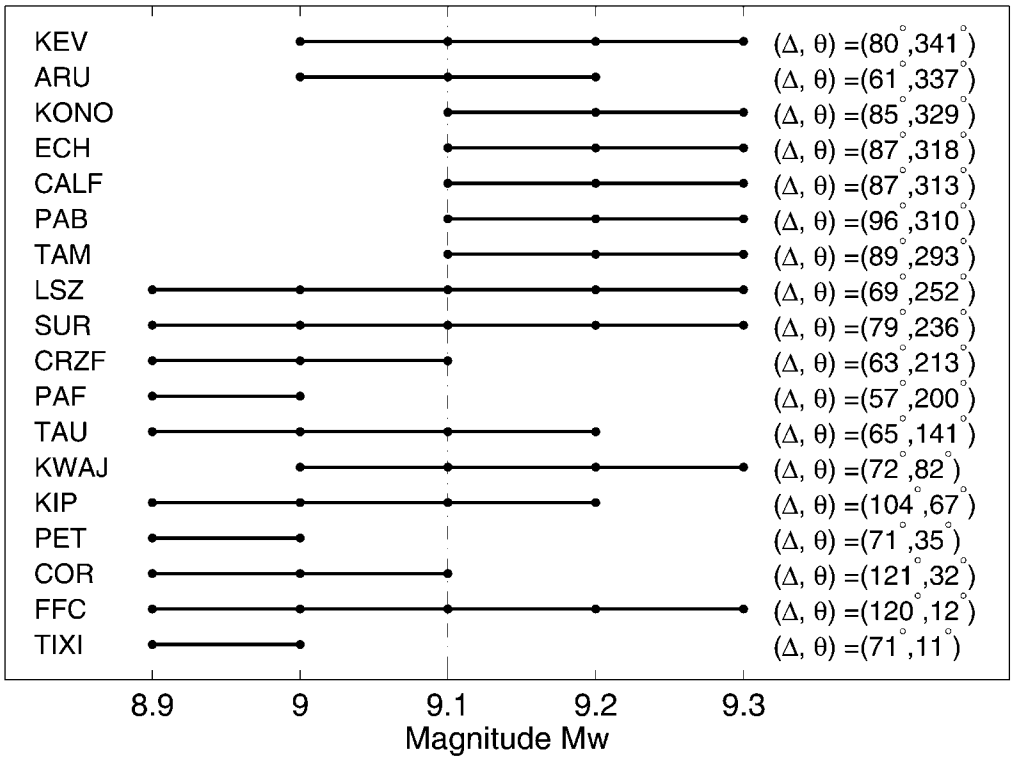

Figure 6. Optimal magnitude of the Sumatra earthquake given by 18 stations of the global network. Station names and their geographical position (epicentral distance Δ and azimuth θ) are specified. At each station, the horizontal line shows the possible magnitude values, according to the criteria described in Figure 5 for stations COR and KONO. The magnitude 9.1 hypothesis is in agreement with most stations (15 of 18) and is therefore the most likely one.

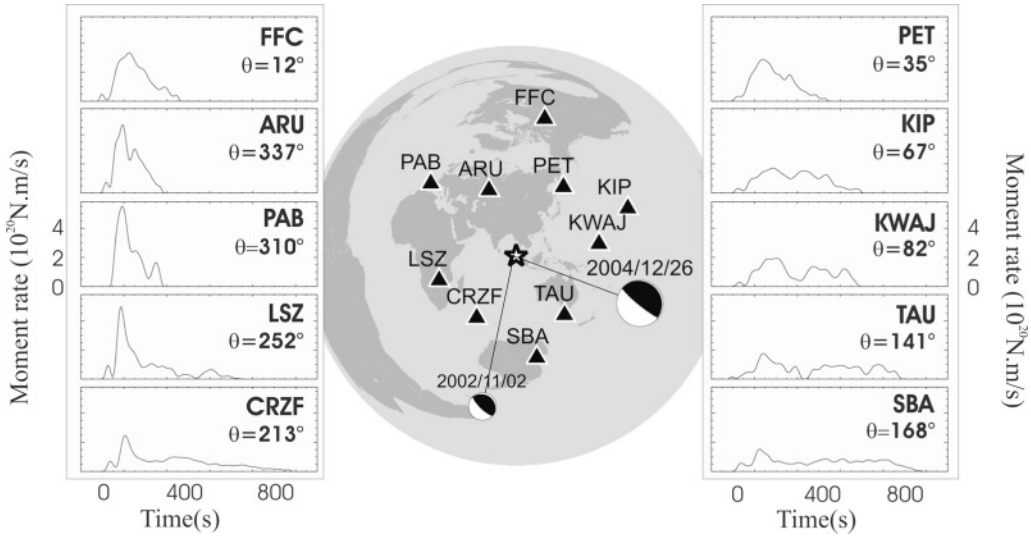

Figure 7. Map of selected seismic sensors (GSN and Geoscope networks) and moment rates (RSTFs) at each station. Harvard CMT (Harvard Seismology, 2004) mechanisms are specified for the mainshock and the EGF. Each RSTF has been obtained by deconvolution of surface waves (Rayleigh waves) between the mainshock of 26 December 2004 and the smaller earthquake (EGF) of 2 November 2002. Station names and azimuths to the north (θ) are specified. Note the much longer and less-impulsive RSTFs for stations to the south than for stations to the north.

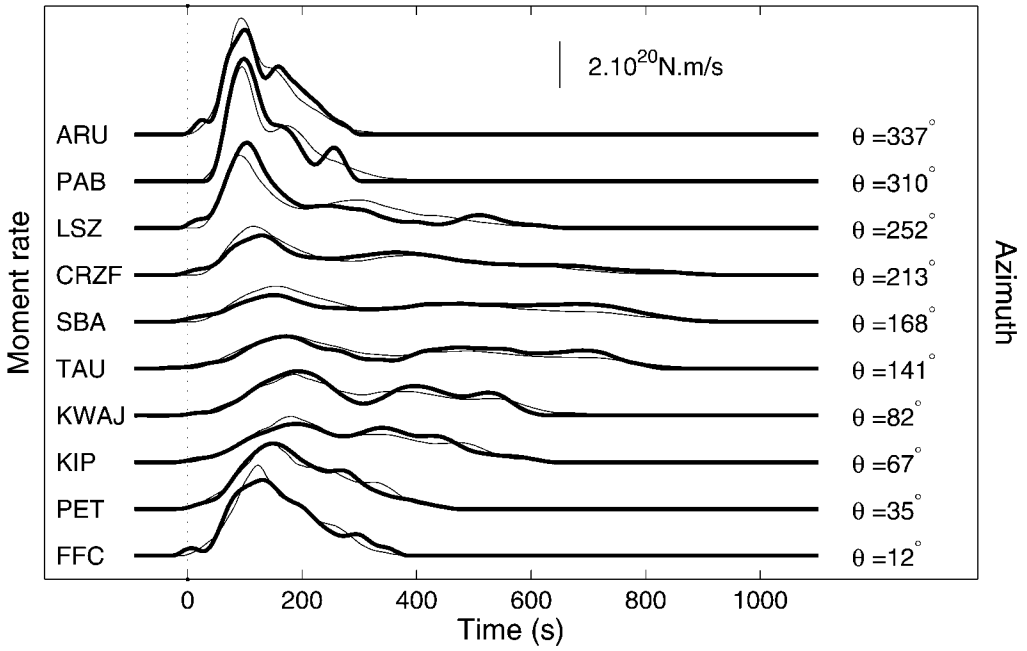

Figure 8. Agreement between observed (thick lines) and synthetic (thin lines) RSTFs as a function of the azimuth θ. Compared to Figure 7, observed RSTFs have been smoothed to reduce the effect of unreliable high frequencies and to take into account the spatial sampling (100 km) of the fault chosen in the simulation. Because of rupture propagation toward north, smoothing is dependent on the azimuth, ranging from 26 sec for $\theta = 337°$ (ARU, directive station) to 134 sec for $\theta = 168°$ (SBA, antidirective station). Synthetic RSTFs, corresponding to the average model (Fig. 9), are in good agreement with the observed ones.

9. In Figure 8, synthetics corresponding to this average model are presented and compared with the observed RSTFs. It can be seen that the apparent duration and main features of each RSTF are well explained by the synthetic model. Moment per unit length and rupture velocity are not very well resolved close to hypocenter due to the line source approximation and the large influence of parameter d in the early part of the rupture. Elsewhere, models are very consistent from one inversion run to the other. Moment per unit length is found even more stable than rupture velocity. Standard errors of rupture velocity become logically large for distances longer 1200 km, where moment release is very low.

Moment per unit length can be converted to slip if rigidity and fault width are known. Taking a fault width equal to 150 km (Bilham *et al.*, 2005) and a classical rigidity equal to 3×10^{10} N m^{-2}, we present in Figure 10 the fault-slip distribution in the Sumatra–Andaman subduction zone. Slip reached values of the order of 20 m 200 km northwest of hypocenter. A secondary slip maximum of about 10 m occurred at Nicobar Islands, and slip remains large (>5 m) up to the South Andaman Islands. Rupture velocity is slow at the beginning (~1.8 km/sec) but this can also be due to our line source approximation that can be wrong in the early part (two-dimensional rupture propagation effects). Then, rupture accelerates to values of 2.4–2.5 km/sec for the next 500 km, before decelerating to 2 km/sec in the second half of the rupture process. Average rupture velocity is equal to 2.2 km/sec (± 0.1) and global duration to 580s (± 20 sec). The main characteristics of the Sumatra earthquake are shown in the map presented in Figure 10.

Conclusions and Discussion

From a methodological point of view, this study has confirmed the very broad range of application of the EGF technique. This method has been used until now on very different earthquake scales, from $M_w \sim 2$ earthquakes (e.g., Fischer, 2005) to $M_w \sim 8$ earthquakes (e.g., Courboulex *et al.*, 1997). It is shown here that this approach is also very helpful to deal with $M_w > 9$ earthquakes. The limitations due to the extent of the rupture zone or to changes in fault orientation exist but can be taken into account by an appropriate filtering of the data. This assertion, which is intuitive in terms of seismic wavelengths, has been supported by the direct observation of seismic data in the Sumatra and Mexican subduction zones. An adaptation of the EGF technique is also proposed to search the optimal moment ratio between the mainshock and the EGF. In the Sumatra case, where the EGF moment is well known, such an approach has provided a simple and independent way to estimate the Sumatra mainshock moment. In other contexts, for example, if one wants

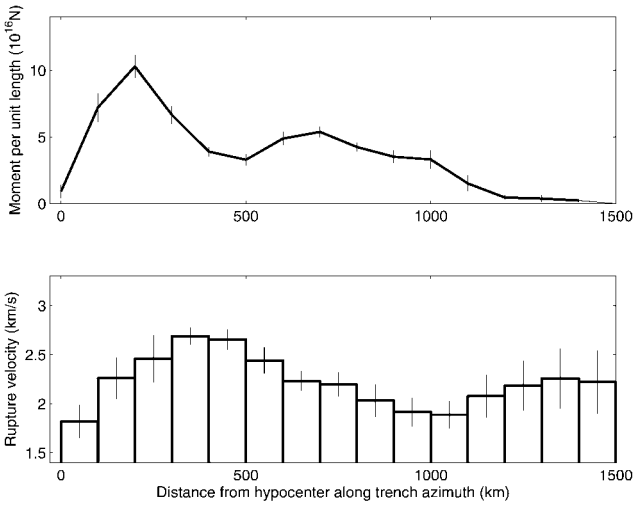

Figure 9. Moment distribution and rupture velocity models. Average models—based on 12 runs of NA with different tuning parameters—are presented in the upper part for moment per unit length and in the lower part for rupture velocity. Uncertainities corresponding to ($\pm\sigma$) are shown by vertical bars. The resolution for moment is good except for the region between Nicobar and Andaman islands (~1000 km from hypocenter) where model dispersion is larger. Rupture velocity is better resolved at the beginning of the rupture than in the later part, and the very small moment of the final part of the rupture process (>1200 km) logically results in a larger dispersion of the possible rupture velocities.

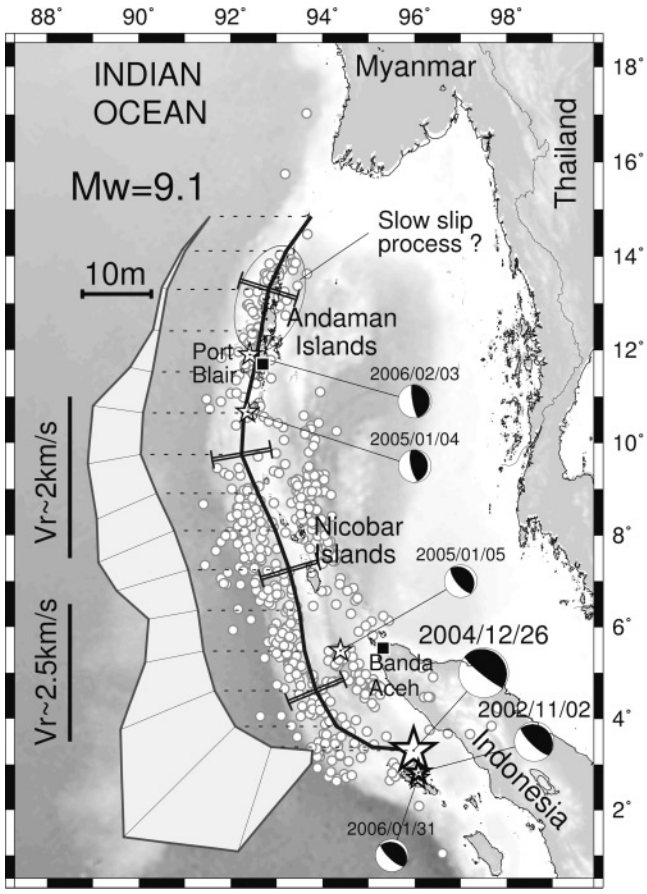

Figure 10. Rupture model of the giant Sumatra earthquake. The rupture extends from the north Sumatra to the south Andaman islands and can be compared with aftershocks occurring in the three days following the earthquake (white circles) (National Earthquake Information Center, 2004). Epicentral location (NEIC, 2004) and Harvard CMT mechanism (Harvard Seismology, 2004) of the mainshock (large thick star), of the EGF (small thick star), and of the four aftershocks used to examine Rayleigh waves consistency (small thin stars) are also shown. Selected fault geometry, represented by the thick black line, follows the trench curvature. Fault width, taken equal to 150 km (Bilham *et al.*, 2005), is shown with black lines perpendicular to the trench, assuming that fault dip is 15°. The average slip model along the trench (deduced from average model of Figure 9 and the 150-km-wide fault) is presented in the left part of the figure, shifted horizontally with respect to the fault position. Slip values have to be read along the thin line perpendicular to the local fault azimuth, according to the scale written above the slip model. Main features of the rupture velocity behavior are presented on the left of the slip model. Slow-slip process may have occurred in the central and north Andaman Islands, where seismic moment release is very low.

to determine the magnitude of small events, the technique can also be used in the opposite direction: given the optimal moment ratio and the magnitude of the mainshock, the magnitude of a small EGF can be estimated.

The giant Sumatra earthquake, as imaged by very broadband Rayleigh waves (100–2000 sec), has a seismic moment equal to 5.6×10^{22} N m (M_w 9.1). The earthquake dynamically ruptured a 1100- to 1200-km long segment of the Sumatra–Andaman trench, and this process lasted about 580 sec ($\pm$20 s). This value is far beyond any earthquake rupture duration defined until now. For example, duration of the M_w 9.2 1964 Alaska earthquake has been estimated to 240 sec (Alaska Earthquake Information Center, 2005). Using the EGF analysis, the first 200 sec of the rupture are found to be very energetic, with a maximum slip of 20 m occurring 200 km away from the hypocenter, close to the bend of the trench (Ji, 2005). A secondary maximum is identified close to Nicobar Islands, with slip of about 10 m, and seismic rupture has kept propagating toward north up to the South Andaman Islands. This behavior is similar to the one derived from seismological data (Ammon *et al.*, 2005; Lay *et al.*, 2005), GPS data (Chlieh *et al.*, 2007), or tsumami data (Piatanesi and Lorito, 2007). Rupture velocity is everywhere—except at hypocenter—of the order of, or larger than, 2 km/sec, even if slower velocities have been allowed in the

inversion. The average value is found equal to 2.2 km/sec, in agreement with most studies, which have defined this parameter between 2 and 2.5 km/sec (Ammon *et al.*, 2005; de Groot-Hedlin, 2005; Guilbert *et al.*, 2005; Lomax, 2005). More precisely, rupture velocity has reached a value of ~2.5 km/sec in the segment between Sumatra and Nicobar Islands, before slowing down to ~2 km/sec in the late part of the rupture.

The moment of 5.6×10^{22} N m defined by Rayleigh waves is close to the value found by much longer period data. For example, Park *et al.* (2005) by normal mode study, or Banerjee *et al.* (2005) with geodetical data and a realistic dip of the trench, have retrieved a value of $6–6.5 \times 10^{22}$ N m. This means that if slow slip exists, it is of the order of 10%–20% of the global moment released by the earthquake. This low value can also explain why Vigny *et al.* (2005) have not detected some slow process in their GPS data. Our study find large slip (10 m) in the Nicobar region, which is approximately the value required by subsidence observation (Bilham *et al.*, 2005). Thus, no longer does timescale slip seem required in this part of the fault. Andaman Islands region is a different case. Except in the southern part, the modeled moment release is very low, whereas there has been some evidence of fault activity: aftershock sequence is dense up to 14° N, subsidence has been observed in the western shorelines of Andaman Islands (Bilham *et al.*, 2005), and GPS analysis seems to require significant slip in this zone. For compatibily of these observations we propose here that the slow-slip process, if present, has to be confined in the extreme north of the rupture zone, between 12° and 14° N.

Acknowledgments

I am grateful to the Federation of Digital Seismic Networks (FDSN) and to Geoscope and TGRS networks for free and easy access to broadband data. Revisions proposed by two anonymous reviewers and discussions inside Geosciences Azur laboratory have greatly contributed to improve the manuscript. Generic Mapping Tools (GMT) free software has been helpful to the preparation of the manuscript.

References

Aki, K. (1967). Scaling law of seismic spectrum, *J. Geophys. Res.* **72,** 1217–1231.

Alaska Earthquake Information Center (2005). The great Alaska earthquake of 1964, www.giseis.alaska.edu/quakes/Alaska_1964_earthquake.html (last accessed).

Ammon, C. J., C. Ji, H.-K. Thio, D. Robinson, S. Ni, V. Hjorleifsdottir, H. Kanamori, T. Lay, S. Das, D. Helmberger, G. Ichinose, J. Polet, and D. Wald (2005). Rupture process of the 2004 Sumatra–Andaman earthquake, *Science* **308,** 1133–1139.

Ammon, C. J., A. A. Velasco, and T. Lay (1993). Rapid estimation of rupture directivity: application to the 1992 Landers (Ms = 7.4) and Cape Mendocino (Ms = 7.2), California earthquakes, *Geophys. Res. Lett.* **20,** 97–100.

Banerjee, P., F. F. Pollitz, and R. Burgmann (2005). The size and duration of the Sumatra–Andaman earthquake from far-field static offsets, *Science* **308,** 1769–1772.

Bertero, M., D. Bindi, P. Boccacci, M. Cattaneo, C. Eva, and V. Lanza (1997). Application of the projected Landweber method to the estimation of the source time function in seismology, *Inverse Problems* **13,** 465–486.

Bilham, R., E. R. Engdahl, N. Feldl, and S. P. Satyabala (2005). Partial and complete rupture of the Indo-Andaman plate boundary 1847–2004, *Seism. Res. Lett.* **76,** 299–311.

CESS Seismology Research Group (2005). Preliminary estimates of the geodetic GPS survey in the Andaman & Nicobar Islands conducted by CESS, http://www.seires.net/content/view/122/52/ (last accessed).

Chlieh, M., J. P. Avouac, V. Hjorleifsdottir, T. R. A. Song, C. Ji, K. Sieh, A. Sladen, H. Hebert, L. Prawirodirdjo, Y. Bock, and J. Galetzka (2007). Coseismic slip and afterslip of the great (M_w 9.15) Sumatra–Andaman Earthquake of 2004, *Bull. Seism. Soc. Am.* **97,** no. 1A, ●●●–●●●.

Courboulex, F., S. K. Singh, J. Pacheco, and C. Ammon (1997). The October 9, 1995 Colima-Jalisco, Mexico, earthquake (Mw 8): a study of the rupture process, *Geophys. Res. Lett.* **24,** 1019–1022.

Courboulex, F., J. Virieux, A. Deschamps, D. Gibert, and A. Zollo (1996). Source investigation of a small event using empirical Green's functions and simulated annealing, *Geophys. J. Int.* **125,** 768–780.

de Groot-Hedlin, C. D. (2005). Estimation of the rupture length and velocity of the Great Sumatra earthquake of Dec 26, 2004 using hydroacoustic signals, *Geophys. Res. Lett.* **32,** L11303, doi 10.1029/2005GL022695.

Department of Civil Engineering (2005). Indian Institute of Technology Kanpur, Quick Report on the Study of the 2004 Sumatra Earthquake and Tsunami Effects, http://cires.colorado.edu/~bilham/IndonesiAndaman2004_files/KanpurMalek.pdf. (last accessed).

Fischer, T. (2005). Modelling of multiple events using empirical Green's functions: method, application to swarm earthquakes, and implications for their rupture propagation, *Geophys. J. Int.* **163,** 991–1005.

Fukuyama, E., and K. Irikura (1986). Rupture process of the 1983 Japan Sea (Akita-Oki) earthquake using a waveform inversion method, *Bull. Seism. Soc. Am.* **76,** 1623–1640.

Guilbert, J., J. Vergoz, E. Schisselé, A. Roueff, and Y. Cansi (2005). Use of hydroacoustic and seismic arrays to observe rupture propagation and source extent of the M_w 9.0 Sumatra earthquake, *Geophys. Res. Lett.* **32,** L15310, doi 10.1029/2005GL022966.

Hartzell, S. H. (1978). Earthquake aftershocks as Green's functions, *Geophys. Res. Lett.* **5,** 1–4.

Harvard Seismology. Centroid Moment Tensor catalog search, www.seismology.harvard.edu/ (last accessed).

Heaton, T. (1990). Evidence for and implications of self-healing pulses of slip in earthquake rupture, *Phys. Earth. Planet. Interiors* **64,** 1–10.

Ihmlé, P. F (1996). Frequency dependent relocation of the 1992 Nicaragua slow earthquake: an empirical Green's function approach, *Geophys. J. Int.* **127,** 75–85.

Ihmlé, P. F., and J. C. Ruegg (1997). Source tomography by simulated annealing using broad-band surface waves and geodetic data: application to the Mw = 8.1 Chile 1995 event, *Geophys. J. Int.* **131,** 146–158.

Ishii, M., P. Shearer, H. Houston, and J. E. Vidale (2005). Extent, duration and speed of the 2004 Sumatra–Andaman earthquake imaged by the Hi-Net array, *Nature* **435,** 933–936.

Ji, C. (2005). Magnitude 9.0 off the west coast of northern Sumatra Sunday, December 26, 2004 at 00:58:53 UTC, Preliminary rupture model, http://neic.usgs.gov/neis/eq_depot/2004/eq_041226/neic_slav_ff.html (last accessed)

Krüger, F., and M. Ohrnberger (2005). Tracking the rupture of the M_w = 9.3 Sumatra earthquake over 1,150 km at teleseismic distance, *Nature* **435,** 937–939.

Lambotte, S., L. Rivera, and J. Hinderer (2007). Constraining the overall kinematics of the 2004 Sumatra and the 2005 Nias earthquakes using the Earth's gravest free oscillations, *Bull. Seism. Soc. Am.* **97,** no. 1A, ●●●–●●●.

Lay, T., H. Kanamori, C. J. Ammon, M. Nettles, S. N. Ward, R. C. Aster, S. L. Beck, S. L. Bilek, M. R. Brudzinski, R. Butler, H. R. DeShon, G. Ekstrom, K. Satake, and S. Sipkin (2005). The great Sumatra–Andaman earthquake of 26 December 2004, *Science* **308,** 1127–1133.

Lomax, A. (2005). Rapid estimation of rupture extent for large earthquakes: application to the 2004, M9 Sumatra–Andaman mega-thrust, *Geophys. Res. Lett*. **32,** L10314, doi 10.1029/2005GL022437.

Mori, J., and A. Frankel (1990). Source parameters for small events associated with the 1986 North Palm Springs, California, earthquake determined using empirical Green functions, *Bull. Seism. Soc. Am*. **80,** 278–295.

Mueller, C. S. (1985). Source pulse enhancement by deconvolution of an empirical Green's function, *Geophys. Res. Lett.* **12,** 33–36.

National Earthquake Information Center (2004). http://neic.usgs.gov/neis/epic/. (last accessed).

Ni, S., H. Kanamori, and D. Helmberger (2005). High frequency radiation from the 2004 Great Sumatra–Andaman earthquake, *Nature* **434,** 582.

Park, J., T.-R. A. Song, J. Tromp, E. Okal, S. Stein, G. Roult, E. Clevede, G. Laske, H. Kanamori, P. Davis, J. Berger, C. Braitenberg, M. Van Camp, X. Lei, H. Sun, H. Xu, and S. Rosat (2005). Earth's free oscillations excited by the 26 December 2004 Sumatra–Andaman earthquake, *Science* **308,** 1139–1144.

Piatanesi, A., and S. Lorito (2007). Rupture process of the 2004 Sumatra–Andaman earthquake from tsunami waveforms inversion, *Bull. Seism. Soc. Am.* **97,** no. lA, ●●●–●●●.

Sambridge, M. (1999). Geophysical inversion with a neighborhood algorithm. I. Searching a parameter space, *Geophys J. Int.* **138,** 479–494.

Stein, S., and E. Okal (2005). Ultra-long period seismic moment of the great December 26, 2004 Sumatra earthquake and implications for the slip process, *Nature* **434,** 581.

Survey of India (2005). http://news.indiainfo.com/2005/01/15/1501survey.html (last accessed).

Vallée, M. (2004). Stabilizing the empirical Green function analysis: development of the projected Landweber method, *Bull. Seism. Soc. Am.* **94,** 394–409.

Vallée, M., and M. Bouchon (2004). Imaging coseismic rupture in far field by slip patches, *Geophys. J. Int.* **156,** 615–630.

Velasco, A. A., C. J. Ammon, and T. Lay (1994). Empirical Green function deconvolution of broadband surface waves: rupture directivity of the 1992 Landers, California (Mw = 7.3), *Bull. Seism. Soc. Am.* **84,** 735–750.

Vigny, C., W. Simons, S. Abu, R. Bamphenyu, C. Satirapod, N. Choosakul, C. Subarya, A. Socquet, K. Omar, H. Abidin, and B. A. C. Ambrosius (2005). Insight into the 2004 Sumatra–Andaman earthquake from GPS measurements in southeast Asia, *Nature* **436,** 201–206.

Yagi, Y. (2004). Preliminary results of rupture process for 2004 off coast of northern Sumatra giant earthquake, http://iisee.kenken.go.jp/staff/yagi/eq/Sumatra2004/Sumatra2004.html (last accessed).

Yamanaka, Y. (2004). 04/12/26 off West coast of northern Sumatra, EIC Seismological Note No.161, www.eri.u-tokyo.ac.jp/sanchu/Seismo Note/2004/EIC161e.html (last accessed).

Géosciences Azur, IRD
250 avenue Albert Einstein
06560 Valbonne, France

Manuscript received 16 January 2006.